Nuclear Science and Techniques (2025) 36:214
https://doi.org/10.1007/s41365-025-01783-4

STARE: a new detector array for exploring the breakup reaction mechanisms induced by weakly bound nuclei

Yan-Song Wu[1] · Gao-Long Zhang[1] · Cheng-Jian Lin[2] · Nan-Ru Ma[2] · Lei Yang[2] · Guang-Xin Zhang[3] · Shi-Peng Hu[4,5] · Huan-Qiao Zhang[2] · Marco Mazzocco[6,7] · Yong-Jin Yao[1] · Zhen-Wei Jiao[1] · Ming-Li Wang[1] · Xue-Dou Su[1] · Hao-Bo Lv[1] · Kun Dong[1]

Received: 13 March 2025 / Revised: 21 May 2025 / Accepted: 11 June 2025 / Published online: 21 August 2025

Abstract
A new detector array with a large solid angle coverage for the coincidence measurement of charged fragments was developed to study the breakup reaction mechanisms of weakly bound nuclear systems at energies around the Coulomb barrier. The array has been used to explore the breakup reaction mechanisms of ^{6,7}Li + ^{209}Bi systems at $E_{\mathrm{beam}} = 30, 40, 47$ MeV, showing good performance in particle identification and complete kinematic measurements. Based on this, different breakup modes and breakup components were clearly distinguished, and some new breakup modes were discovered, such as $^{7}\mathrm{Li} \rightarrow \alpha + t$ breakup mode in ^{6}Li + ^{209}Bi system and $^{7}\mathrm{Li} \rightarrow {}^{6}\mathrm{He} + p$ breakup mode in ^{7}Li + ^{209}Bi system. This array can also be used to explore other breakup reaction mechanisms induced by weakly bound nuclei.

Keywords Detector array · Coincidence measurement · Breakup reaction · Weakly bound nuclei

1 Introduction

Nuclear reactions at energies near the Coulomb barrier are effective for studying the interactions between the nuclear structure and dynamics. As more exotic weakly bound nuclei become accessible at new accelerator facilities, the measurement of reaction cross sections for weakly bound nuclear systems at sub-barrier energies is of great interest [1–3]. At present, it is found that in reactions involving these weakly bound nuclei, compared with theoretical calculations and tightly bound nuclei, complete fusion is significantly suppressed at energies above the Coulomb barrier and a remarkable enhancement at energies below the Coulomb barrier [4–8]. To investigate the breakup effects of weakly bound nuclei on the suppression of the complete fusion cross section, the study of the breakup reaction and mechanism of weakly bound nuclei is crucial importance [9–15].

Compared to a radioactive ion beam (RIB), the beam intensities of stable weakly bound nuclei such as ^{6,7}Li and ^{9}Be are orders of magnitude higher [16]. Several silicon

This work was supported by the National Key R&D Program of China (Nos. 2022YFA1602302 and 2023YFA1606402), the National Natural Science Foundation of China (Nos. U2167204, 12175314, 12235020 and 12275360), the Continuous-Support Basic Scientific Research Project and the "111 Center", and the China Scholarship Council (CSC).

✉ Gao-Long Zhang
zgl@buaa.edu.cn

Cheng-Jian Lin
cjlin@ciae.ac.cn

[1] School of Physics, Beihang University, Beijing 100191, China

[2] China Institute of Atomic Energy, Beijing 102413, China

[3] Sino-French Institute of Nuclear Engineering and Technology, Sun Yat-Sen University, Zhuhai 519082, China

[4] Institute for Advanced Study in Nuclear Energy and Safety, Shenzhen University, Shenzhen 518060, China

[5] Shenzhen Key Laboratory of Research and Manufacture of High Purity Germanium Materials and Detectors, Shenzhen University, Shenzhen 518060, China

[6] Dipartimento di Fisica e Astronomia, Università di Padova, 35131 Padova, Italy

[7] Istituto Nazionale di Fisica Nucleare, Sezione di Padova, 35131 Padova, Italy

detector arrays, such as EXPADES [17], GLORIA [18], and MITA [19], have recently been built to study the breakup mechanism induced by these stable weakly bound nuclei. Along with the identification of some breakup modes, the breakup effect of these nuclei on the fusion process has been preliminarily studied [20]. However, owing to the limited coverage angle of the previously mentioned detector arrays and the complexity of the breakup modes, it is challenging to detect rare breakup events and obtain the angular distribution of different breakup products.

In view of this fact, a new Silicon Telescopic Array for Reactions induced by Exotic nuclei (STARE), designed by the China Institute of Atomic Energy (CIAE), was employed for the coincidence measurement of charged fragments induced by weakly bound nuclei at energies around the Coulomb barrier. Compared with previous arrays [17–19], STARE incorporates more telescope detectors, providing larger solid-angle coverage and improved particle identification, which enables the detection of new breakup modes with small cross-sections. In addition, a specially designed frame allows both STARE and preamplifiers to be mounted directly inside the chamber, thereby simplifying the installation and reducing noise. The coincidence measurement of ^{6,7}Li + ^{209}Bi at E_{beam} = 30, 40, 47 MeV was carried out successfully in the CIAE by STARE. In this study, the innovation features and performance of STARE, as well as the methods and preliminary results of the data analysis, are described in detail.

2 Description of the array

The STARE consists of eight telescope units, as shown in Fig. 1a. Each telescope unit consists of (i) a double-sided silicon strip detector (DSSD) with a thickness of 40 µm for backward angles and 60 µm for forward angles, and (ii) a quadrant silicon detector (QSD) with a thickness of 1000 µm. To avoid the light charged particles not being clearly identified in the Δ E vs. E spectrum at forward angles due to their low energy loss in the DSSD, an additional QSD with a thickness of 300 µm was inserted between the DSSD and the 1000 µm thick QSD at forward angles. A brief description of this detector array is provided in Refs. [13, 21]. The eight telescope units surrounding the target were installed on a designed frame produced by 3D printing, which makes the array lighter and easy to be carried. The relative positions of the telescope units and the target are summarized in Table 1. As shown in Fig. 1b, the array covers polar angles θ_{lab} from 25° to 155°, and spans 301° in azimuthal angle, occupying 26.8% of the 4π sr. A larger number of telescope units provide larger solid angle coverage, greatly improving the coincidence detection efficiency compared with previous experiments [22–25].

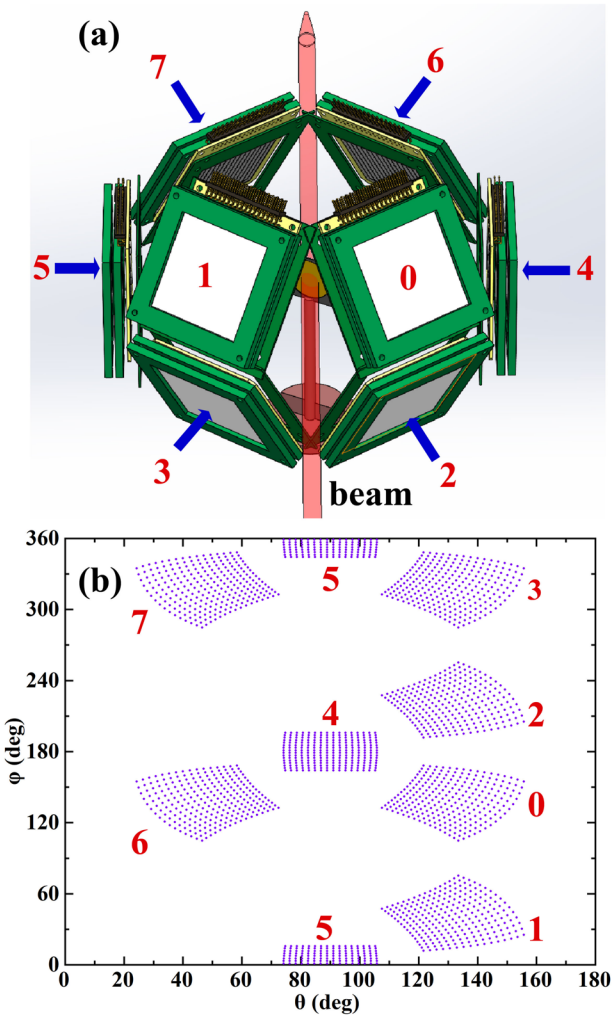

Fig. 1 (Color online) **a** The arrangement of the detector array of eight telescopes with respect to the beam direction (arrow from bottom to top). **b** Angular coverage of detector array, pixel separation in each DSSD is exaggerated for clarity

Table 1 The information of different telescope units

Unit No.	Distance between unit and target (mm)	The angle of the center of each unit (θ, ϕ)
0	70	132.1°, 139.2°
1	70	132.1°, 40.8°
2	70	132.1°, 220.8°
3	70	132.1°, 319.2°
4	82	90°, 180°
5	82	90°, 0°
6	70	47.9°, 139.2°
7	70	47.9°, 319.2°

A mylar foil with a thickness of 0.5 μm was installed in front of the telescope to stop low-energy electrons. As illustrated in Fig. 1a, the compact structure enables the installation of the mylar foil and silicon detectors as close as possible to each other with the lowest energy loss and angular straggling. Moreover, the integrated preamplifiers designed by CIAE [26] were installed in close proximity to the detectors and positioned in the target chamber to reduce noise. To ensure stable operation of the preamplifiers, a cooling system is employed to dissipate the heat of the electronics and reduce the detector leakage current. Specifically, two brass rings are mounted on the top and bottom of the detector array, and all preamplifiers are fixed to these brass rings. During the experiments, the brass rings were cooled using a dedicated cooling system that provided a stable and low-temperature operating environment for the preamplifiers. These preamplifiers have been applied in several experiments and exhibit excellent and stable performance [27–34]. A specific photograph is shown in Fig. 2.

Silicon detectors are widely used owing to their high detection efficiency and good energy resolution [35]. In STARE, the kinetic energy of the particles was obtained from the energy signal of the pixel of the DSSDs, with a resolution of 100–150 keV FWHM for ~5 MeV α sources. To provide supporting evidence, Fig. 3 presents the energy spectra of the α sources measured using DSSDs of 40, 60 μm. The energy resolutions of the peaks corresponding to ^{239}Pu were determined to be ~2.0%, ~1.8%, respectively. For the same α source, the energy resolution of the QSD is approximately 0.5%. The width of each strip of the DSSD was 3 mm, and the size of each pixel of the DSSD was 3 mm × 3 mm. Figure 1b shows the scattering angles of the centers of all DSSD pixels. We can infer that the angular resolution in the central region of each pixel of the DSSDs is approximately ±1.5°, with an improved resolution observed in the peripheral regions of the detector telescopes in the laboratory frame. Complete kinematic measurements can be performed with good energy and angular resolution, which are important for describing the breakup process.

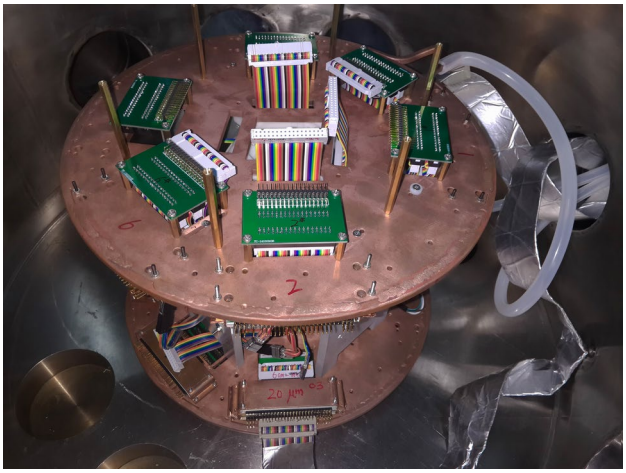

Fig. 2 (Color online) Photograph of the detector array with preamplifiers and cooling rings

3 Experiment

Coincident measurements with beams of ^{6,7}Li were conducted at the HI-13 tandem accelerator of the CIAE. The beam energies at the center of the ^{209}Bi target (210 μg/cm^2 thick self-supporting) were approximately E_{beam} = 30, 40, 47 MeV. A collimator with a diameter of 3 mm was positioned 30 cm upstream of the target, aligned along the beam axis, to precisely define the beam spot size and position. The target was fixed at the center of STARE with a normal angle of 70° relative to the beam line to minimize the dead area caused by the target frame. Four silicon detectors were installed at a distance of 250 mm from the center of the target for beam monitoring. To minimize the data collection rate during breakup measurements, the data were recorded when at least two pixels of the entire detector array were hit by particles in the multi-hit trigger mode.

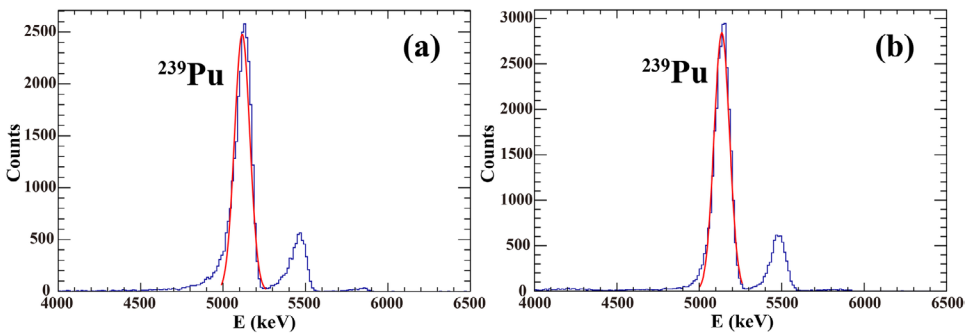

Fig. 3 (Color online) The energy spectra of the α sources measured by DSSDs of STARE. **a** from 40 μm DSSD, **b** from 60 μm DSSD

4 Data analysis

4.1 Energy calibration

Energy calibration of the DSSDs was carried out using two α sources (^{239}Pu, ^{241}Am), and the α particles decayed from the products of the fusion reactions. Additionally, energy calibrations of the QSDs were performed by evaluating the deposited energies of the charged particles within the QSDs. This was achieved by subtracting the measured energy loss in the DSSDs from the expected particle energy, as determined by calculations using the reference for LISE++. In the experiment, the coordinate location of the DSSDs pixels was used to determine the scattering angle of the charged particles detected by the detectors. A typical energy-calibrated single spectrum for ^{7}Li + ^{209}Bi measured at E_{beam} = 40 MeV is presented in Fig. 4, which shows elastic scattering events at ~36 MeV. For reactions in normal kinematics that produce two nuclei in the final state, such as elastic scattering or transfer, the energy of a projectile-like nucleus decreases monotonically with θ. The α lines between 5 and 10 MeV, as shown in Fig. 4, with energies independent of the angle, originate from the evaporation residues formed following complete fusion (CF) and incomplete fusion (ICF).

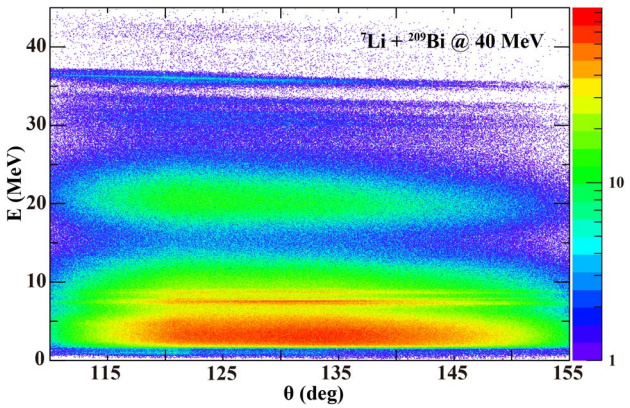

Fig. 4 (Color online) Energy-calibrated single spectrum for ^{7}Li + ^{209}Bi measured at E_{beam} = 40 MeV and displayed across the angular coverage of No.0-3 telescope units

4.2 Removal of spurious events

According to the principle of DSSDs, we used the energy signal output from both sides of the DSSDs (marked E_{loss1}, E_{loss2}, respectively) to select the correct events. As shown in Fig. 5a, considering the statistics of events and the proportion of accidental coincidences, we select the events with E_{loss1} - E_{loss2} distributed within the σ (~100 keV) widening range as correct events. The two-dimensional spectrum E_{loss1} vs. E_{loss2} after screening is shown in Fig. 5b. During the experiment, a large number of particles hit the inter-strips of the DSSDs, leading to a non-negligible number of accidental coincidence events (~3%). The two-dimensional spectra of the particles depositing energy in adjacent strips of the same DSSD before and after screening based on (a) are illustrated in Fig. 5c and

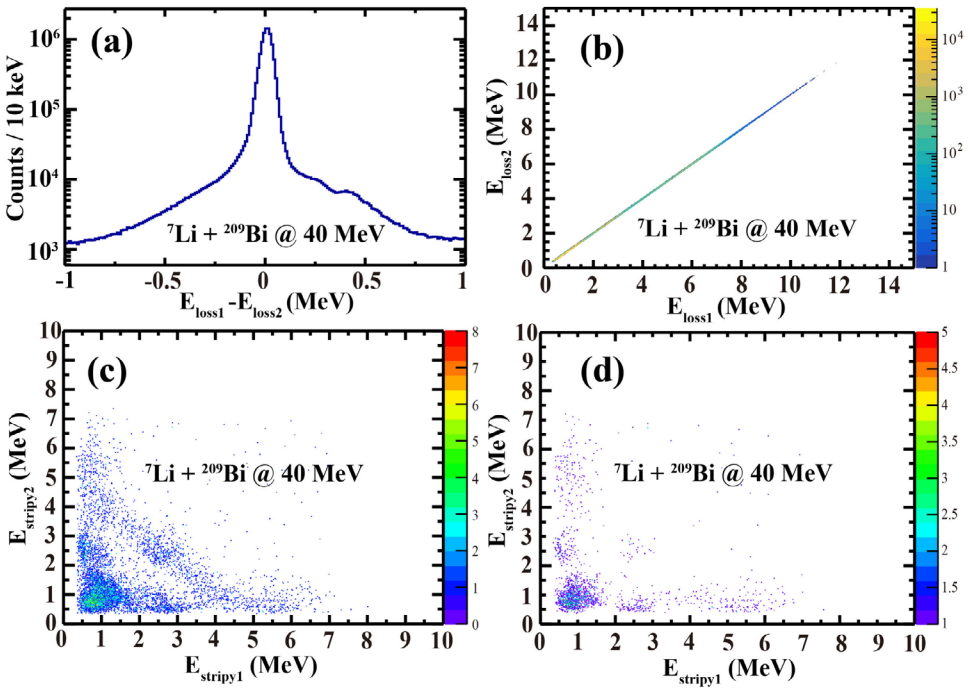

Fig. 5 (Color online) Example of No.0-3 telescope unit to demonstrate accidental events removal from ^{7}Li + ^{209}Bi at E_{beam} = 40 MeV. **a** The single energy spectrum of the difference in energy loss between the two sides of DSSD. **b** The two-dimensional energy spectrum E_{loss1} vs. E_{loss2} of the two sides of DSSD after screening based on **a**. **c**, **d** Particle energy deposition on adjacent silicon strips in the same side of DSSD before and after screening based on **a**

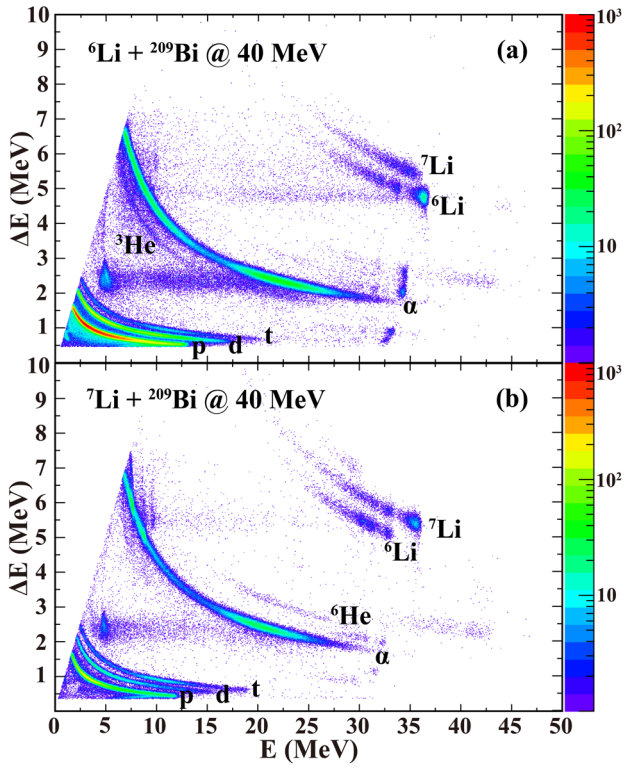

Fig. 6 (Color online) Calibrated two-dimensional ΔE - E particle identification spectra by No.2 telescope unit which covers an angular range from 110° to 155°. **a** for ^{6}Li + ^{209}Bi at E_{beam} = 40 MeV, **b** for ^{7}Li + ^{209}Bi at E_{beam} = 40 MeV

d. In Fig. 5c, inter-strip events mainly originate from α, p, d, t particles distributed on the different lines $y = -x + c$. These events were removed after energy screening of the DSSDs, as shown in Fig. 5d.

Typical two-dimensional particle identification spectra obtained from the same telescope unit are shown in Fig. 6. Owing to the excellent energy resolution of the detectors and statistics, the different masses (A = 1–7) and charges (Z = 1–3) produced by the different reaction channels can be clearly identified. In particular, the ^{3}He and ^{6}He bands can be observed in the experimental data of ^{6,7}Li, which provides the possibility of observing new breakup modes. In Fig. 6a, ^{7}Li band can be observed. It is evident that ^{6}Li picked up one neutron from the target; thus, 1n-pickup process induced by ^{6}Li can occur. In Fig. 6b, ^{6}Li band can be observed. This is due to 1n-stripping of ^{7}Li. The results show that 1n-stripping process is populated in the reactions of ^{7}Li. The other light particles were analyzed in sections below.

4.3 Identification of breakup modes

During the breakup process, momentum conservation dictates that the total momentum of the fragments should remain zero in the center of mass frame of the projectile-like nucleus. Thus, fragments must travel in opposite directions in the center of the mass frame but may be emitted in any direction. As a result, we can filter out α particles from the breakup process, as shown in Fig. 7a, from ^{6}Li + ^{209}Bi at E_{beam} = 40 MeV, when a continuous distribution of energies with maximum and minimum energies is given by

$$E_{\mathrm{min,max}} = \frac{m_1}{m_1 + m_2}\left(E_{\mathrm{p}} + \frac{m_2}{m_1}Q_{\mathrm{BU}} \pm 2\sqrt{\frac{m_2}{m_1}Q_{\mathrm{BU}}E_{\mathrm{p}}}\right), \quad (1)$$

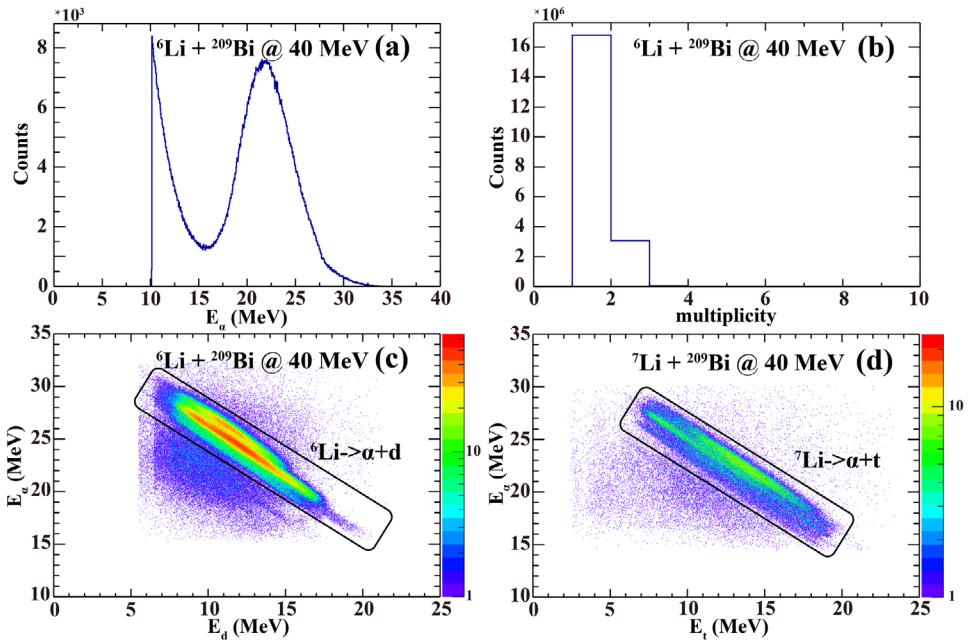

Fig. 7 (Color online) **a** Single energy spectrum of inclusive α from No.0-3 telescope units. **b** Particle multiplicity of the entire array. **c**, **d** The two-dimensional energy spectrum of the direct breakup modes from ^{6,7}Li at E_{beam} = 40 MeV

E_p is the projectile-like fragment energy prior to breakup, m_i is the mass of the breakup fragments, and Q_{BU} is the Q -value for the breakup process. Figure 7b shows the current particle multiplicity (the number of particles contained in a coincidence event). We can observe that inclusive elastic scattering or transfer events still account for the majority, and the rest are the two coincidence fragments we expected.

The correlations between the kinetic energies of the coincident fragments from the direct breakup mode of ^{6,7}Li at $E_{beam} = 40$ MeV are presented in Fig. 7c and d. The band-like structures are immediately obvious, which suggests that these events have originated from the true $^6\text{Li} \rightarrow \alpha + d$ and $^7\text{Li} \rightarrow \alpha + t$ breakup processes. Other breakup events from different modes can be extracted in the same manner.

Based on the extracted breakup events, two-body dynamics calculations can be used to reconstruct the breakup reaction Q value to further understand the breakup mechanism. The energy change (Q value) in the reaction can be determined by Eq. (2):

$$Q = E_1 + E_2 + E_{rec} - E_{lab}. \tag{2}$$

E_1, E_2 are the kinetic energies of the coincidence particles in the reactions. E_{rec} is the energy of the recoiling target-like nucleus determined by conservation of momentum in three body system. E_{lab} is the laboratory kinetic energy of the incident projectile (E_{beam} for energy loss in the target after correcting). The ground-state Q value (Q_{gg}), for any collision can be expressed by:

$$Q_{gg} = E_p + E_{p,x} + E_{rec} + E_{t,x} - E_{lab}, \tag{3}$$

where E_p is the kinetic energy of projectile-like nuclei and $E_{p,x}$ and $E_{t,x}$ are the excitation energies of projectile-like nuclei and target-like nuclei, respectively. For binary breakup, $E_p + E_{p,x} = E_1 + E_2$. Therefore, the Q spectra provide more information for each state populated in the target-like nucleus (calculated using $E_{t,x} = Q_{gg}$ - Q).

The reconstructed Q spectra of all the breakup modes in the reactions of ^{6,7}Li with ^{209}Bi at $E_{beam} = 30$, 40 and 47 MeV are shown in Fig. 8. Vertical dashed lines indicate the expected Q_{gg}, which corresponds to the ground state of the target-like nucleus. In the reaction of ^{6}Li, compared with the direct breakup mode ($^6\text{Li} \rightarrow \alpha + d$), the breakup of ^{5}Li into $\alpha + p$ after 1n-stripping seems to be the most dominant, as can also be verified in Refs. [23, 36, 37]. In addition, a new breakup mode, $^7\text{Li} \rightarrow \alpha + t$ was observed for the first time by STARE with obvious Q value peaks, indicating the ground and excited states of ^{208}Bi. We can observe that the relevance of the $^7\text{Li} \rightarrow \alpha + t$ channel increases with beam energy. The discovery of $^7\text{Li} \rightarrow \alpha + t$ breakup mode indicates that the 1n-pickup process cannot be ignored in the reaction of ^{6}Li, which also provides an additional explanation for the origin of inclusive α particles [38, 39].

For the reaction ^{7}Li + ^{209}Bi, the breakup triggered by a 1p-pickup is the most probable channel for ^{7}Li. The breakup after the production of ^{8}Be into two α particles produces multiple peaks in the Q value spectra, including the ground state and two excited states of ^{208}Pb. However, when the target is replaced by a medium-mass nucleus, conclusions may be inconsistent. In the ^{7}Li + ^{93}Nb system [40], $\alpha + t$ and $\alpha + d$ are dominant. When the beam energy was increased to 40, 47 MeV, despite a very high breakup threshold (~10 MeV), a significant number of $^6\text{He} + p$ events were observed in ^{7}Li + ^{209}Bi system. The present exclusive measurement of ^{6}He in coincidence with a proton that provides direct evidence of the $^6\text{He} + p$ cluster configuration of ^{7}Li is important for understanding the possible nuclear cluster structures of ^{7}Li [41].

4.4 Prompt breakup vs. resonant breakup

In recent works [25, 36], the relative energy (E_{rel}) of breakup fragments has been reported to provide significant information on the breakup time-scale and to allow a classification of the breakup process into prompt breakup or resonant breakup, which can be expressed in terms of the measured energies and masses of the fragments, and the measured opening angle of the fragments within the laboratory frame (θ_{12}):

$$E_{rel} = \frac{m_2 E_1 + m_1 E_2 - 2\sqrt{m_1 E_1 m_2 E_2}\cos\theta_{12}}{m_1 + m_2}. \tag{4}$$

As presented in Fig. 9a and b, the E_{rel} distribution of ^{209}Bi(^{6}Li,^{6}Li→ α+d)^{209}Bi and ^{209}Bi(^{7}Li,^{7}Li→ α+t)^{209}Bi at $E_{beam} = 40$ MeV is peaking around at ~0.7 and ~2.1 MeV, which correspond to the resonant states of ^{6}Li (3^+, 2.186 MeV) and ^{7}Li ($7/2^-$, 4.63 MeV), respectively. These peaks are associated with the breakup on the outgoing trajectory, which is not affected by the target-like Coulomb field and can be described as a resonant breakup. On the other hand, when the lifetime of the final state in the projectile-like nucleus is lower than the breakup scale (~10^{-22} s), breakup will occur in the entrance channel close to the target-like nucleus (prompt breakup) with a smooth and continuous E_{rel} distribution as a consequence of the Coulomb interaction exerted by the target-like nucleus. To better identify the different breakup components experimentally, new insights were focused on the angular correlation spectra. As shown in Fig. 9c and d, the expected correlation between β and θ_{12} for resonant breakup from $^6\text{Li} \rightarrow \alpha + d$ and $^7\text{Li} \rightarrow \alpha + t$ corresponds well to the red solid lines, which confirms the interpretation of these events breakup far from the target-like nucleus. β is the orientation of the relative velocity of the fragments with respect to the motion of their center of mass, as determined by Eq. (5). v_i and u_i are the velocities of each fragment in the laboratory and their center-of-mass frame, respectively. A schematic of the relationship between these

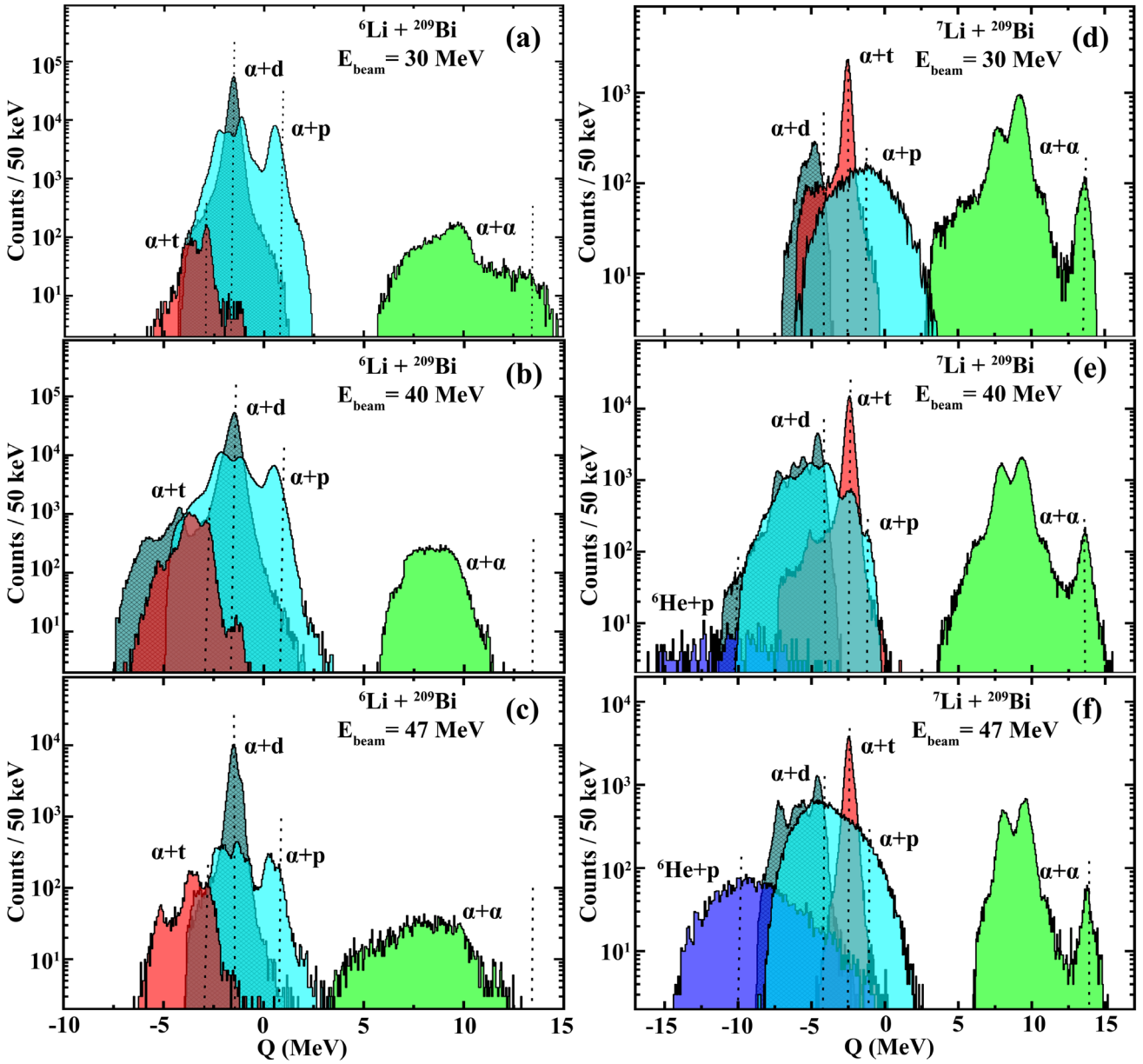

Fig. 8 (Color online) The Q value spectra determined for ^{6,7}Li + ^{209}Bi at E_{beam} = 30, 40, 47 MeV including different breakup modes, the vertical dashed lines indicate the expected Q_{gg} for each breakup mode in reactions of ^{6}Li and ^{7}Li, respectively

variables is shown in the upper right corner of Fig. 9d. For events arising from breakup near the target-like that correspond to the prompt breakup, the β vs. θ_{12} correlation is distorted owing the influence of Coulomb interaction on the fragment trajectories. The prompt and resonant breakup components can be distinguished well by the relative energy spectrum and angular correlation spectrum calculated using STRAE.

$$\sin\beta = \frac{v_1 v_2 \sin\theta_{12}}{\sqrt{v_2^2 u_1^2 + v_1^2 u_2^2 + 2u_1 u_2 v_1 v_2 \cos\theta_{12}}} \tag{5}$$

5 Summary

In this study, a new multilayer silicon telescope array was designed and manufactured to study the breakup reaction mechanisms induced by weakly bound nuclear systems at energies around the Coulomb barrier. In the new array,

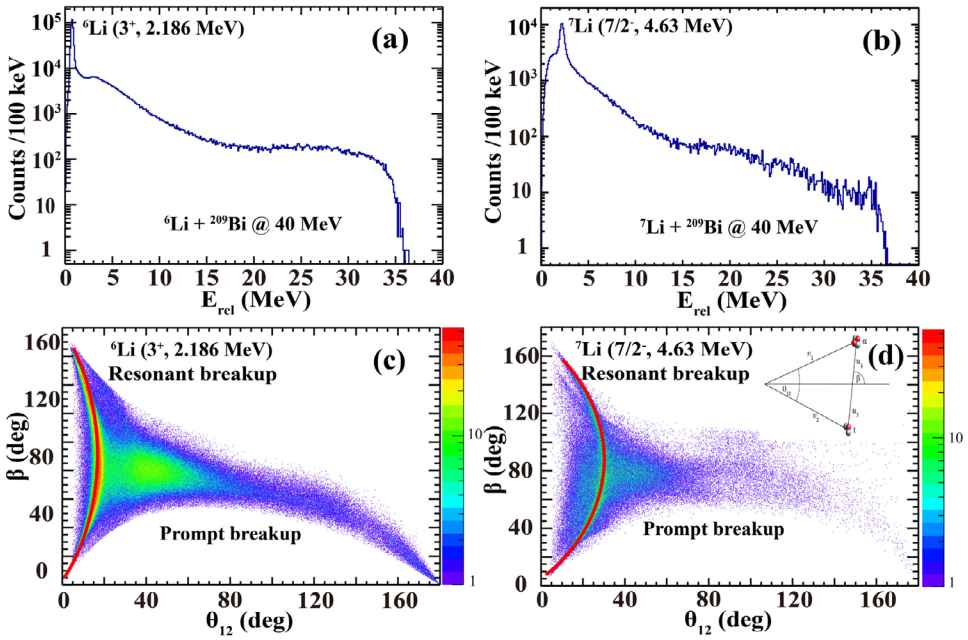

Fig. 9 (Color online) **a**, **b** Distributions of the relative energy of the coincident breakup fragments in direct breakup modes induced by ^{6,7}Li + ^{209}Bi at E_{beam} = 40 MeV. **c**, **d** The β vs. θ_{12} spectra of breakup pairs for ^{6,7}Li + ^{209}Bi at E_{beam} = 40 MeV. Solid lines show the expected β vs. θ_{12} correlation assuming resonant breakup from the long-lived 3^{+} resonant state in ^{6}Li and 7/2^{-} resonant state in ^{7}Li

integrated preamplifiers are positioned near the detectors and operate continuously and stably in a low-temperature environment, which is very important for reducing noise. STARE with a large solid angle greatly improves the coincidence efficiency, making it possible to collect breakup events with very small cross-sections.

STARE has been successfully used to investigate the coincidence measurement of charged fragments in ^{6,7}Li + ^{209}Bi systems at E_{beam} = 30, 40, 47 MeV. Owing to the powerful particle identification and energy resolution of STARE, different breakup modes can be clearly distinguished by two-body dynamics calculations, along with the observation of new breakup modes. Different breakup components (prompt breakup and resonant breakup) can be identified by the relative energy and angular correlation spectra, which are important for reproducing the breakup process of weakly bound nuclei. To facilitate the understanding of the breakup mechanisms of weakly bound nuclei and to elucidate the cluster structure within the projectile-like nucleus, the angular distributions of different breakup components are currently being pursued. Simultaneously, our collaborators are also trying to develop a theoretical framework for predicting these reactions. The details of this work are presented in a forthcoming paper.

Acknowledgements We are grateful to the CIAE staff for providing a stable ^{6,7}Li beam throughout the experiments.

Author Contributions All authors contributed to the study conception and design. Material preparation, data collection and analysis were performed by Yan-Song Wu, Gao-Long Zhang, Cheng-Jian Lin, Nan-Ru Ma, Lei Yang, Yong-Jin Yao. The first draft of the manuscript was written by Yan-Song Wu, and all authors commented on previous versions of the manuscript. All authors read and approved the final manuscript.

Data Availability The data that support the findings of this study are openly available in Science Data Bank at https://cstr.cn/31253.11.sciencedb.27318 and https://doi.org/10.57760/sciencedb.27318.

Declarations

Conflict of interest The authors declare that they have no Conflict of interest.

References

1. E.F. Aguilera, P.A. Valenzuela, E. Martinez-Quiroz et al., Near-barrier fusion of the ^{6}B + ^{58}Ni proton-halo system. Phys. Rev. Lett. **107**, 092701 (2011). https://doi.org/10.1103/PhysRevLett.107.092701
2. L.F. Canto, P.R.S. Gomes, R. Donangelo et al., Recent developments in fusion and direct reactions with weakly bound nuclei. Phys. Rep. **596**, 1–86 (2015). https://doi.org/10.1016/j.physrep.2015.08.001
3. X.P. Yang, G.L. Zhang, H.Q. Zhang, Systematic study of reaction functions of weakly bound nuclei. Phys. Rev. C **87**, 014603 (2013). https://doi.org/10.1103/PhysRevC.87.014603
4. S.P. Hu, G.L. Zhang, J.C. Yang et al., Small suppression of the complete fusion of the ^{6}Li + ^{96}Zr system at near-barrier energies. Phys. Rev. C **91**, 044619 (2015). https://doi.org/10.1103/PhysRevC.91.044619
5. Y.D. Fang, P.R.S. Gomes, J. Lubian et al., Complete and incomplete fusion of ^{9}Be + ^{169}Tm, ^{187}Re at near-barrier energies. Phys. Rev. C **91**, 014608 (2015). https://doi.org/10.1103/PhysRevC.91.014608

6. C.L. Guo, G.L. Zhang, S.P. Hu et al., Coupling effects on the fusion of ^{6}Li + ^{154}Sm at energies slightly above the Coulomb barrier. Phys. Rev. C **92**, 014615 (2015). https://doi.org/10.1103/PhysRevC.92.014615
7. M.F. Guo, G.L. Zhang, P.R.S. Gomes et al., Negligible suppression of the complete fusion of ^{6,7}Li on light targets, at energies above the barrier. Phys. Rev. C **94**, 044615 (2016). https://doi.org/10.1103/PhysRevC.94.044605
8. G.S. Li, J.G. Wang, J. Lubian et al., Fusion reactions in the ^{9}Be + ^{197}Au system above the Coulomb barrier. Phys. Rev. C **100**, 054601 (2019). https://doi.org/10.1103/PhysRevC.100.054601
9. E.F. Aguilera, J.J. Kolata, F.M. Nunes et al., Transfer and/or breakup modes in the ^{6}He + ^{209}Bi reaction near the coulomb barrier. Phys. Rev. Lett. **84**, 5058–5061 (2000). https://doi.org/10.1103/PhysRevLett.84.5058
10. M. Dasgupta, P.R.S. Gomes, D.J. Hinde et al., Effect of breakup on the fusion of ^{6}Li, ^{7}Li, and ^{9}Be with heavy nuclei. Phys. Rev. C **70**, 024606 (2004). https://doi.org/10.1103/PhysRevC.70.024606
11. L. Jin, A.M. Moro, Numerical assessment of post-prior equivalence for inclusive breakup reactions. Phys. Rev. C **92**, 061602 (2015). https://doi.org/10.1103/PhysRevC.92.061602
12. L. Jin, A.M. Moro, Comprehensive analysis of large α yields observed in ^{6}Li-induced reactions. Phys. Rev. C **95**, 044605 (2017). https://doi.org/10.1103/PhysRevC.95.044605
13. Y.J. Yao, C.J. Lin, L. Yang et al., Relative probabilities of breakup channels in reactions of ^{6,7}Li with ^{209}Bi at energies around and above the Coulomb barrier. Chin. Phys. C **45**, 054104 (2021). https://doi.org/10.1088/1674-1137/abe3ee
14. L. Yang, C.J. Lin, H. Yamaguchi et al., Breakup of the proton halo nucleus ^{8}B near barrier energies. Nat. Commun. **13**, 7193 (2022). https://doi.org/10.1038/s41467-022-34767-8
15. G.L. Zhang, Z.W. Jiao, G.X. Zhang et al., Further investigation on the fusion of ^{6}Li with ^{209}Bi target at near-barrier energies. Chin. Phys. C **48**, 074001 (2024). https://doi.org/10.1088/1674-1137/ad4264
16. S.P. Hu, G.L. Zhang, G.X. Zhang et al., A powerful combination measurement for exploring the fusion reaction mechanisms induced by weakly bound nuclei. Nucl. Instr. Methods Phys. Res. A **914**, 64–68 (2019). https://doi.org/10.1016/j.nima.2018.05.067
17. M. Romoli, E. Vardaci, A. Anastasio et al., EXPADES: a new detection system for charged particles in experiments with RIBs. Nucl. Instr. Methods Phys. Res. B **266**, 4637–4642 (2008). https://doi.org/10.1016/j.nimb.2008.05.121
18. G. Marquínez-Durán, L. Acosta, R. Berjillos et al., GLORIA: a compact detector system for studying heavy ion reactions using radioactive beams. Nucl. Instr. Methods Phys. Res. A **755**, 69–77 (2014). https://doi.org/10.1016/j.nima.2014.04.002
19. N.R. Ma, L. Yang, C.J. Lin et al., MITA: a Multilayer Ionization-chamber Telescope Array for low-energy reactions with exotic nuclei. Eur. Phys. J. A **55**, 1–11 (2019). https://doi.org/10.1140/epja/i2019-12765-7
20. L. Yang, C.J. Lin, N.R. Ma et al., Breakup dynamics of weakly bound nuclei at energies around the Coulomb barrier. Fundamental Res. (2023). https://doi.org/10.1016/j.fmre.2023.10.006
21. Y.J. Yao, C.J. Lin, L. Yang et al., The effects of beam drifts on elastic scattering measured by the large solid-angle covered detector array. Nucl. Sci. Tech. **32**, 14 (2021). https://doi.org/10.1007/s41365-021-00854-6
22. R. Rafiei, R. Rietz, D.H. Luong et al., Mechanisms and systematics of breakup in reactions of ^{9}Be near-barrier energies. Phys. Rev. C **81**, 024601 (2010). https://doi.org/10.1103/PhysRevC.81.024601
23. D.H. Luong, M. Dasgupta, D.J. Hinde et al., Predominance of transfer in triggering breakup in sub-barrier reactions of ^{6,7}Li with ^{144}Sm, ^{207,208}Pb, and ^{209}Bi. Phys. Rev. C **88**, 034609 (2013). https://doi.org/10.1103/PhysRevC.88.034609
24. S. Santra, V.V. Parkar, K. Ramachandran et al., Resonant breakup of ^{6}Li by ^{209}Bi. Phys. Lett. B **677**, 139–144 (2009). https://doi.org/10.1016/j.physletb.2009.05.016
25. E.C. Sunil Kalkal, D.H.L. Simpson et al., Asymptotic and near-target direct breakup of ^{6}Li and ^{7}Li. Phys. Rev. C **93**, 044605 (2016). https://doi.org/10.1103/PhysRevC.93.044605
26. D.X. Wang, C.J. Lin, L. Yang et al., Compact 16-channel integrated charge-sensitive preamplifier module for silicon strip detectors. Nucl. Sci. Tech. **31**, 48 (2020). https://doi.org/10.1007/s41365-020-00755-0
27. L.J. Sun, X.X. Xu, C.J. Lin et al., A detection system for charged-particle decay studies with a continuous-implantation method. Nucl. Instr. Methods Phys. Res. A **804**, 1–7 (2015). https://doi.org/10.1016/j.nima.2015.09.0390
28. L.J. Sun, X.X. Xu, D.Q. Fang et al., β-decay study of the $T_z = -2$ proton-rich nucleus ^{20}Mg. Phys. Rev. C **95**, 014314 (2017). https://doi.org/10.1103/PhysRevC.95.014314
29. X.X. Xu, C.J. Lin, L.J. Sun et al., Observation of β-delayed two-proton emission in the decay of ^{22}Si. Phys. Lett. B **766**, 312–316 (2017). https://doi.org/10.1016/j.physletb.2017.01.028
30. L. Yang, C.J. Lin, H.M. Jia et al., Optical model potentials for ^{6}He + ^{64}Zn from ^{63}Cu(^{7}Li,^{6}He)^{64}Zn reactions. Phys. Rev. C **95**, 034616 (2017). https://doi.org/10.1103/PhysRevC.95.034616
31. L. Yang, C.J. Lin, H.M. Jia et al., Abnormal behavior of the optical potential for the halo nuclear system ^{6}He + ^{209}Bi. Phys. Rev. C **96**, 044615 (2017). https://doi.org/10.1103/PhysRevC.96.044615
32. L. Yang, C.J. Lin, H.M. Jia et al., Is the dispersion relation applicable for exotic nuclear systems? the abnormal threshold anomaly in the ^{6}He + ^{209}Bi system. Phys. Rev. Lett. **119**, 042503 (2017). https://doi.org/10.1103/PhysRevLett.119.042503
33. G.L. Zhang, Y.J. Yao, G.X. Zhang et al., A detector setup for the measurement of angular distribution of heavy-ion elastic scattering with low energy on RIBLL. Nucl. Sci. Tech. **28**, 104 (2017). https://doi.org/10.1007/s41365-017-0249-0
34. G.X. Zhang, G.L. Zhang, C.J. Lin et al., The calibration of elastic scattering angular distribution at low energies on HIRFL-RIBLL. Nucl. Instr. Methods Phys. Res. A **846**, 23–28 (2017). https://doi.org/10.1016/j.nima.2016.11.058
35. X.X. Xu, F.C.E. Teh, C.J. Lin et al., Characterization of CIAE developed double-sided silicon strip detector for charged particles. Nucl. Sci. Tech. **29**, 73 (2018). https://doi.org/10.1007/s41365-018-0406-0
36. D.H. Luong, M. Dasgupta, D.J. Hinde et al., Insights into the mechanisms and time-scales of breakup of ^{6,7}Li. Phys. Lett. B **695**, 105–109 (2011). https://doi.org/10.1016/j.physletb.2010.11.007
37. G.L. Zhang, Z.W. Jiao, G.X. Zhang et al., One-neutron stripping process in the ^{209}Bi(^{6}Li,^{5}Li)^{210}Bi* reaction. Nucl. Sci. Tech. **35**, 104 (2024). https://doi.org/10.1007/s41365-024-01462-w
38. C. Signorini, A. Edifizi, M. Mazzocco et al., Exclusive breakup of ^{6}Li by ^{208}Pb at Coulomb barrier energies. Phys. Rev. C **67**, 044607 (2003). https://doi.org/10.1103/PhysRevC.67.044607
39. S. Santra, S. Kailas, V.V. Parkar et al., Disentangling reaction mechanisms for α production in the ^{6}Li + ^{209}Bi reaction. Phys. Rev. C **85**, 014612 (2012). https://doi.org/10.1103/PhysRevC.85.014612
40. S.K. Pandit, A. Shrivastava, K. Mahata et al., Probing transfer to unbound states of the ejectile with weakly bound ^{7}Li on ^{93}Nb. Phys. Rev. C **93**, 061602 (2016). https://doi.org/10.1103/PhysRevC.93.061602

41. D. Chattopadhyay, S. Santra, A. Pal et al., Role of cluster structure in the breakup of ^{7}Li. Phys. Rev. C **97**, 051601 (2018). https://doi.org/10.1103/PhysRevC.97.051601